Advances in Continuous and Discrete Models

RESEARCH Open Access

Estimating the two consecutive epidemic waves of SARS-CoV-2 Omicron in Shenzhen, China from November 2022 to July 2023: a modeling study based on multi-source surveillance and mobility data

Yepeng Shi[1,2†], Qiuying Lv[3,4†], Kemin Zhu[1], Jun Cai[5], Dongfeng Kong[3], Kang Liu[1], Zhigao Chen[3], Zhen Zhang[3*] and Ling Yin[1,6*]

*Correspondence:
yinling@siat.ac.cn;
zhangzhen@wjw.sz.gov.cn
[1]Shenzhen Institutes of Advanced Technology, Chinese Academy of Sciences, Shenzhen, China
[3]Department of Communicable Diseases Control and Prevention, Shenzhen Center for Disease Control and Prevention, Shenzhen 518055, China
Full list of author information is available at the end of the article
†Yepeng Shi and Qiuying Lv, as the first authors, contributed equally to this article.

Abstract

Unlike many countries that have experienced multiple COVID-19 waves since January 2020, China's stringent measures left most of the population without natural immunity to SARS-CoV-2. After lifting controls, China experienced two distinct Omicron waves from November 2022 to July 2023. However, no reliable study has yet elucidated the transmission dynamics of these two consecutive Omicron waves in China's megacities, nor the phenomenon of reinfection due to immune escape. To address this gap, this study proposes a hybrid epidemic modeling framework based on multi-source surveillance and mobility data, including nucleic acid tests, wastewater surveillance, case reports from Notifiable Infectious Diseases Surveillance System of China (NIDSS), and intra-urban travel intensity data. In this hybrid modeling framework, a four-stage compartmental model stratified by age is developed, integrating human mobility and Omicron reinfection mechanisms. This model is further corrected by an agent-based model to address the overestimation of infections by the compartmental model, forming a comprehensive hybrid framework. Based on the simulation results, several new findings are drawn. The attack rate of the first wave in Shenzhen was 88.5% (95% confidence interval (CI): 72.1%-99.6%), lower than other models' predictions. The peak of the second wave occurred on May 18, 2023, with a higher reinfection rate compared to those observed in other countries and regions. The effective reproduction number (R_t) for the first wave peaked at 5.44 (95% CI: 5.26-5.48), while for the second wave, the initial R_t was 1.28 (95% CI: 1.27-1.29). The first infections provide a 0.549 (95% CI: 0.544-0.554) protective effect against XBB reinfection within six months. In conlusion, this study presents an advanced modeling framework for accurately assessing epidemic spread in urban environments using multi-source surveillance data.

Keywords: Omicron; Shenzhen; China; Hybrid modeling framework; Reinfection; Mobility; Multi-source surveillance data

1 Introduction

After the outbreak of COVID-19 in late 2019, SARS-CoV-2 rapidly spread globally, leading to a pandemic [1–4]. In response, the Chinese government implemented a stringent "Zero-COVID" policy until November 2022 [5–7]. With growing evidence of the reduced severity of Omicron variants [8], China began gradually adjusting its COVID-19 control policies in November 2022 [9–12]. Since then until July 2023, many areas of China had experienced two consecutive distinct waves of Omicron driven by the major subvariants BA.5/BF.7 and XBB, respectively [13, 14]. Unlike many other countries and regions that experienced multiple COVID-19 waves caused by different SARS-CoV-2 variants since January 2020 [15, 16], China's prolonged strict measures left the vast majority of its population without natural immunity to SARS-CoV-2 before these two Omicron waves. This unique situation provides an opportunity to investigate the relationship between the two consecutive Omicron waves and to understand how immunity from the first wave, driven by Omicron BA.5/BF.7, influenced the subsequent XBB wave. However, few studies have estimated the dynamics of these two waves using reliable real-world data or assessed the protective effect of a prior Omicron infection against reinfection. This study aims to fill this gap.

It is challenging to accurately monitoring infection dynamics for large-scale epidemic outbreaks, such as daily infections, reinfections, attack rate etc. On the one hand, individual tests such as nucleic acid test are impractical for large populations over the whole period of an outbreak; on the other hand, it is difficult to assess the reporting rate of confirmed cases in various medical institutions. Alternative methods have emerged for assessing the spread of the virus, especially for large-scale outbreaks, including wastewater surveillance [17–19] and serological testing [20, 21]. However, serological surveys only reflect past infection status and cannot capture real-time, rapidly changing trends, especially during fast-evolving outbreaks. Meanwhile, wastewater monitoring is easily affected by environmental factors, making it difficult to assess infection numbers accurately. In contrast, epidemic modelling has consistently proven to be an effective tool for assessing and predicting the dynamic spread of infectious diseases using epidemic-related data [22–24]. Regarding the two consecutive Omicron waves from November 2022 to July 2023 in China, Leung et al.[25], Goldberg et al. [26], and Zhang et al. [27], Ma at al. [28] each relied on non-traditionally epidemic-related monitoring data sources, such as transit data, online surveys from China CDC, and Baidu search indices, to develop compartmental models assessing the dynamics of the first wave of Omicron infections in China, Shanxi province, Beijing specifically. However, these studies focused solely on modeling the first wave and did not explore the impact of immunity from the first wave on subsequent waves. Ma et al. [28] predicted that a small peak might occur in Shanxi by the end of April 2023, but they were unable to provide a detailed assessment of the transmission dynamics. Besides, they did not integrate more reliable data sources from medical institutions or CDC departments, such as nucleic acid tests, wastewater surveillance, and case reports from Notifiable Infectious Diseases Surveillance System of China (NIDSS).

Some studies have attempted to simulate the first wave using real-world data and predict the second wave with some assumptions. For instance, Wu et al. [29] utilized vaccine-induced immunity data from Hong Kong to predict the second wave of Omicron in China, while Wang et al. [14] assumed that antibody effectiveness lasts 4–6 months following Omicron infection to predict the infection dynamics of the second wave. These assump-

tions, based on data from other countries or regions, may lead to inaccuracies in projecting the second wave in China. A retrospective modeling study is needed to assess the dynamics of the second wave using real-world data from China. Given that no single data source can fully capture the dynamics of both Omicron waves, effectively integrate multi-source data into the epidemic model is essential. This study aims to provide such an integration framework. Moreover, previous studies [30, 31] have suggested that the commonly-used population-based transmission models, which assume homogeneous mixing of human contacts, tend to overestimate infections, particularly during the final stages of large-scale outbreaks. This study will address this issue by proposing a modeling framework that estimates a more accurate infection scale. In terms of the related findings in epidemiology, according to the cohort study from UK [32], the reinfection rate for XBB observed in epidemiology is between 14-16%. Previous studies [33, 34] indicate that protection from a previous Omicron infection against a new Omicron reinfection has been found to range from 50-90%. However, these findings were obtained after several rounds of SARS-CoV-2 infections, resulting in build-up of immunity in population. In contrast, China presents a pristine natural scenario where the rate of immune evasion is expected to significantly increase, leading to a higher likelihood of reinfection. In terms of the first wave of Omicron in China since November 2022, from the epidemic modelling community, Goldberg et al. [26] estimated the attack rate in the entire China to be 97% (95% CrI: 95%-99%). Leung et al. [25] estimated that Beijing's attack rate reached 92.3% (95% CrI: 91.4%-93.1%) by January 31, 2023, while Zhang et al. [27] estimated that the attack rate for the first wave in Beijing was 97.5% (95% CI: 97.0%-98.0%) as of January 15, 2023. Li et al. [35] used molecular epidemiological analysis, serological surveys, and wastewater surveillance data to analyze the first Omicron wave in Guangdong province, which peaked on January 11, 2023, with a cumulative infection rate of over 90%. Another serological survey found that the IgM+ rate was 87% in Guangzhou [36], which is significantly lower than the aforementioned results [25–27]. For the second wave, with the mathematical models, Wu et al. [29] posited an 80%/90% attack rate for China's first outbreak and, building on this premise, projected an attack rate of 37.63%/32.65% and a peak at July 2, 2023/Aug 15, 2023 for the subsequent national wave. Zheng et al. estimated a reinfection rate of approximately 24.4% in Shanghai based on a cohort study [37]. As we can see, the several existing studies have also not yet reached a consistent result for this unique but important situation in China. Therefore, this study develops a modelling framework that effectively integrates multi-source data to assess two consecutively large-scale epidemic waves at a city level. To the best of our knowledge, it is the first validated mathematical model to estimate and compare the two Omicron waves in a megacity of China after the lifting of the "Zero-COVID" policy in November 2022. This study also estimates the protective effect of a previous Omicron infection against reinfection in the unique context of China. The highlights of this work include:

1) Offering an epidemic hybrid modelling framework based on multi-source monitoring and mobility data, including nucleic acid tests, wastewater surveillance, case reports from NIDSS, and intra-urban travel intensity data. Notably, this study develops a four-stage compartmental model stratified by age, which integrates the reinfection mechanism of Omicron. The transmission rate is modelled by integrating the intra-urban travel intensity and the contact intensity within and outside of households. The contact intensity is further corrected by an equivalent individual-based model (i.e., agent-based model), cor-

recting the overestimation of infection in the compartmental model and forming a hybrid modelling framework. This study offers an advanced modeling example for accurately assessing epidemic spread in urban settings using multi-source surveillance data.
2) Presenting new findings to enhance the understanding of the epidemic characteristics of Omicron in China, including the attack rate, infection peak time, reinfection rate, and the effective reproduction number (R_t) of the two Omicron waves in a megacity of China. These insights contribute to a deeper understanding of Omicron's epidemic characteristics and the protective effect of natural immunity on Omicron reinfection. The epidemiology of this emerging and rapidly evolving coronavirus can help prepare for future emerging infectious disease, including the potential "Disease X".
Overall, this study not only enhances our understanding of the epidemiological characteristics of Omicron variants and the protective effect of natural Omicron infection against reinfection in the Chinese population, but also offers methodological guidance for model-based assessments of future emerging infectious diseases.

2 Methods

2.1 Study area

Shenzhen, a mega-city of China adjacent to Hong Kong with more than 17 million residents, is the youngest and most densely populated city in China with an average age of 32.5 years (https://www.gov.cn). During the first wave of Omicron since November 2022, the population in Shenzhen likely had almost no immunity against Omicron infection. The main virus strains in the first and second Omicron waves in Shenzhen were BA.5/BF.7 and XBB variants, respectively (https://www.chinacdc.cn). This presents a unique opportunity to directly estimate the transmission of Omicron within a young and dense population. Existing studies indicate that the first Omicron wave in China lasted less than a month but had a high infection rate [26]. This meant that a major proportion of the population in Shenzhen acquired immunity almost at the same time, providing protection against Omicron reinfection for a while [38]. Analyzing Shenzhen's two consecutive Omicron waves together can enhance our understanding of the protective effect of natural immunity of Omicron against reinfection in a young and dense population.

2.2 Data

The data used in our study include four main parts: epidemic surveillance data in Shenzhen, intra-urban mobility data, contact matrix data, and Shenzhen demographic data. The intra-urban mobility, contact matrix, and demographic data can help build a fine-structured epidemic model coupled with human mobility, while the epidemic surveillance data can assist in deriving key parameters for the SARS-CoV-2's transmission dynamics.

2.2.1 Epidemic surveillance data

Nucleic acid test data. In November 2022, Shenzhen issued the following regulations in response to the COVID-19 epidemic situation. To enter public transportation facilities (e.g., airports, train stations, bus stations, passenger terminals, subway stations), ride public transportation vehicles (e.g., subway, busses, taxis, ride-hailing cars), or enter enclosed public spaces, individuals must present a negative nucleic acid test certificate valid within 48 hours of the current day, or a nucleic acid sampling certificate (recorded). Medical institutions and testing facilities are required to report positive samples of the SARS-CoV-2

nucleic acid test to NIDSS. The data is not publicly available, but we (Shenzhen CDC) have internal access. Shenzhen continued to conduct large-scale nucleic acid testing from 11/11/2022 to 12/07/2022. During this period, the number of people tested ranged from 16.2 million to 17.31 million, with a testing rate of 92.64% to 98.9%. We use the daily PCR-positive test data for the calibration of our Stage I and II model, which simulates the Pre-opening and Relaxation period (11/11/2022-12/07/2022), when large-scale nucleic acid screening was still conducted in China. *Wastewater Surveillance data.* Shenzhen is the first city in mainland China to establish routine wastewater surveillance (WWS) to monitor the local transmission of SARS-CoV-2 [19]. From December 3, 2022, to the end of January 2023, Shenzhen CDC conducted a survey at six wastewater treatment plants and nine pumping stations in the Futian and Nanshan districts, covering a population of approximately 3.55 million. Based on the wastewater monitoring results from these two districts, we used the peak time of virus concentration in Shenzhen.

Daily reported cases of COVID-19 from medical institutions. Daily reported cases of COVID-19 from medical institutions, including nucleic acid- or antigen-positive patients with SARS-CoV-2 infections, were reported to Shenzhen CDC by NIDSS within 24 hours. The NIDSS covers all public and private medical institutions in Shenzhen (including fever clinics, inpatient departments, community health centers, etc.). Based on the reported results, we have compiled the daily reported COVID-19 cases from May 1 to June 2, 2023.

2.2.2 Intra-urban mobility data

Previous studies [39, 40] have suggested that intra-urban mobility and physical mixing are relevant to the local spread of COVID-19, which could be gauged by the intra-urban travel intensity. The data for intra-urban travel intensity comes from Baidu Migration (https://qianxi.baidu.com). It is defined as the daily standardized ratio between the number of people with a travel more than 500 meters and the resident population of that city. A higher intra-urban travel intensity indicates a higher proportion of the population traveling on a given day. The daily mobility data of Shenzhen used in this study spans from December 7, 2022 to July 31, 2023.

2.2.3 Contact matrix data

The contact matrix for the age-specific transmission model is from a social contact survey. Leung et al. [39] previously conducted a social contact survey in Hong Kong and estimated the contact matrix by age. They divided population contact patterns into non-household and household contacts, each represented by separate contact matrices. Given the geographical proximity and similar lifestyle patterns between Shenzhen and Hong Kong, this study adopts the contact matrix parameters from Hong Kong to build the epidemic model.

2.2.4 Demographic data

This study utilizes demographic data of Shenzhen from the 7th National Population Census of China in 2020. This included detailed information on the permanent resident population of Shenzhen and age distribution (https://www.gov.cn/guoqing/).

2.3 Model and inference

The two consecutive Omicron waves in Shenzhen from November 11, 2022, to July 31, 2023 consist of different stages of control policy and different Omicron strains. To analyze

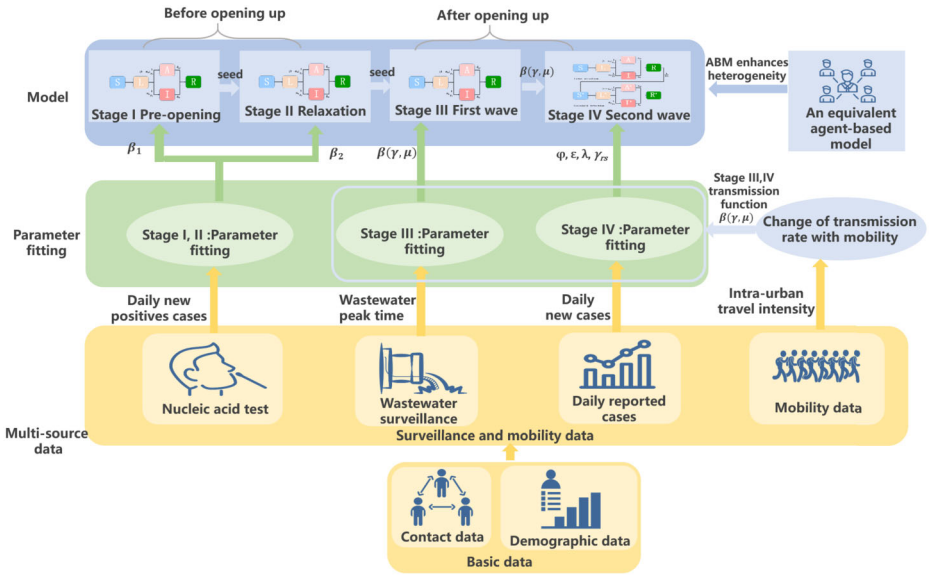

Figure 1 Four-stage hybrid epidemic modeling framework for Omicron in Shenzhen using multi-source surveillance data and mobility data

these two waves, we propose a four-stage modeling framework that effectively leverage different data sources in each stage. Based on the changes in policies and the epidemic situation, the epidemic dynamics are divided into four stages:

1) Stage I Pre-opening (11/11/2022-12/01/2022): On November 11, 2022, the Chinese government announced "20 measures" [9]. Control measures included restricting the control area, reducing the quarantine period for close contacts and inbound individuals, and temporarily halting tracing of secondary contacts.

2) Stage II Relaxation (12/01/2022-12/06/2022): During this period, Shenzhen gradually eased control measures, leading to a gradual increase in the daily new infections.

3) Stage III First Wave (12/07/2022-01/31/2023): On December 7, 2022, the Chinese government issued "10 measures" [10], further promoting individual antigen testing instead of large-scale nucleic acid screening, with individuals voluntarily choosing home quarantine rather than centralized quarantine. From this point, China entered a phase of widespread relaxation.

4) Stage IV Second Wave (02/01/2023-07/31/2023): After the conclusion of the first Omicron wave in Shenzhen, people gradually returned to their pre-pandemic lifestyles. During this stage, individuals who had not been infected in the first wave gradually became infected, and reinfections were observed.

As shown in Figure 1, we construct a four-stage hybrid modeling framework. First, we combine a compartmental model with an agent-based model (ABM) to create a hybrid model that mitigates the traditional compartmental model's tendency to overestimate attack rates [30, 31]. Then, based on the distinct characteristics of each stage of the epidemic and the hybrid model, we establish a Susceptible-Latent-Asymptomatic-Infectious-Removed (SLAIR) model for Stages I to III to simulate the transmission of SARS-CoV-2 in Shenzhen (The "Removed" compartment refers to those who have moved out of the infected system). In the Stage IV, considering the phenomenon of reinfection, a reinfection compartment is introduced into the SLAIR model. Different data are used to fit the

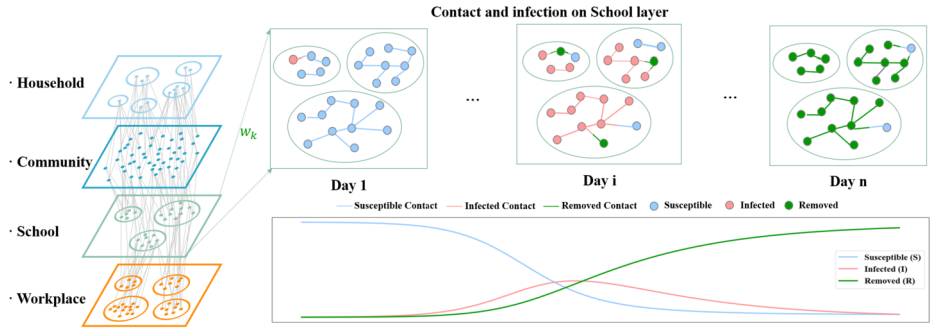

Figure 2 Multi-layer contact and infection spread in an ABM

corresponding parameters. Details of the models and the fitting processes for each stage are discussed in following sections.

2.3.1 The hybrid model combining compartmental model and ABM

ABM can simulate the behaviors and interactions of individual agents with different attributes and actions. This fine-grained modeling can capture the heterogeneity of populations, where individuals may have varying susceptibility and contact rates. In contrast, the core assumption of compartmental model in this study is to use a fixed, age-specific contact matrix to describe population contact patterns. However, this assumption overlooks changes in interpersonal contact patterns and the heterogeneity during the epidemic dynamics [30, 31]. During large-scale outbreaks, we typically focus on the overall infection trends of the population. Compartmental models can quickly assess epidemic dynamics and adjust in real-time based on actual data, whereas ABM requires more computational time.

To leverage the strengths of both models, we develop a hybrid model that integrates the compartmental model and ABM to capture the complex dynamics of epidemic spread. The ABM incorporates a multi-layer contact network encompassing household, workplace, school, and community layers [41, 42]. Each agent within these layers exhibits heterogeneous contact patterns based on real-world statistical data fitted to age-specific and location-specific distributions.As shown in Figure 2, ABM includes four contact layers: Household, Workplace, School, and Community. The figure uses the school contact layer as an example, showing the contact networks on different days (from Day 1 to Day n). The curve chart below shows the trends in the number of susceptible, infected, and removed individuals over time. At each simulation step, the model tracks the total number of susceptible (S) and infected (I) individuals. For each layer k, it calculates the total contact counts $C_{S,k}$, $C_{I,k}$, and $C_{T,k}$ for the susceptible, infected, and total populations, respectively. Using these values, we determine the average contact numbers for the susceptible, infected, and total populations in each layer, denoted as $\mu_{S,k}$, $\mu_{I,k}$, and $\mu_{T,k}$, respectively. These are defined as:

$$\mu_{S,k} = \frac{C_{S,k}}{\mathcal{N}_{S,k}}, \mu_{I,k} = \frac{C_{I,k}}{\mathcal{N}_{I,k}}, \mu_{T,k} = \frac{C_{T,k}}{\mathcal{N}_{T,k}}, \tag{1}$$

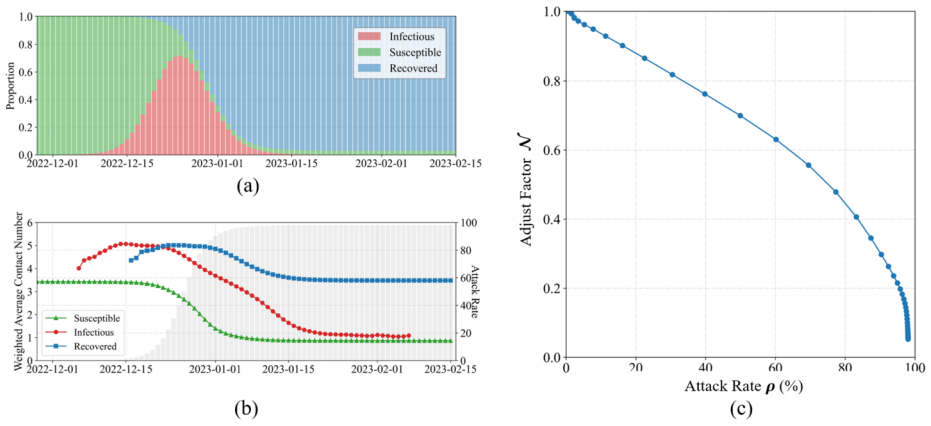

Figure 3 Relationship between the attack rate and the adjustment factor based on the ABM. (a) The proportion of S, I, and R groups over time in the ABM. (b) The average contact numbers of S, I, and R groups in four contact layers. (c) The relationship between the attack rate and the adjustment factor over time

where $\mathcal{N}_{S,k}$, $\mathcal{N}_{I,k}$, and $\mathcal{N}_{T,k}$ represent the number of susceptible individuals, infected individuals, and the total population in layer k, respectively. For example, in Figure 2, on Day i, $C_{S,k}$ is 5, $\mathcal{N}_{S,k}$ is 3 and $\mu_{S,k}$ is $5/3 \approx 1.7$.

The normalized effective transmission contact volume $\mathcal{N}_k$ for each layer is calculated by taking the product of the average contact numbers of S and I and standardizing it by the square of the average contact number of the total population:

$$\mathcal{N}_k = \left(\mu_{S,k} \times \mu_{I,k}\right) / \mu_{T,k.}^2 \tag{2}$$

These normalized volumes from each layer are then aggregated into an overall metric:

$$\mathcal{N} = \sum_k w_k \times \mathcal{N}_k, \tag{3}$$

where w_k represents the predefined weight reflecting the relative importance of contact time in each layer based on survey and time-use data (Appendix A.2).

As shown in Figure 3, in the ABM simulation, the average contact numbers of S, I, and R change as their proportions change. In Fig. 3(b), at the initial stage, due to the small number of I and R, they are filtered out when calculating the average contact numbers. The shaded area represents the trend of the attack rate over time. At each simulation step, we treat the aggregated metric $\mathcal{N}$ as a dependent variable and the attack rate ρ for that day as an independent variable. Here ρ represents the cumulative proportion of infected individuals in the population from the initial time $t = 0$ to the current time t, as shown in Equation (4). This allows us to derive a function $g(\rho)$ representing the relationship between the attack rate and the adjustment factor $\mathcal{N}$. $g(\rho)$ does not have a fixed analytical form, but is instead an empirically derived function based on the results of agent-based model simulations. By simulating daily cumulative infection rates ρ within the ABM and recording the corresponding effective contacts, we created a mapping of $\rho \to \mathcal{N}$ values, which represents the relationship between the attack rate ρ and the adjustment factor

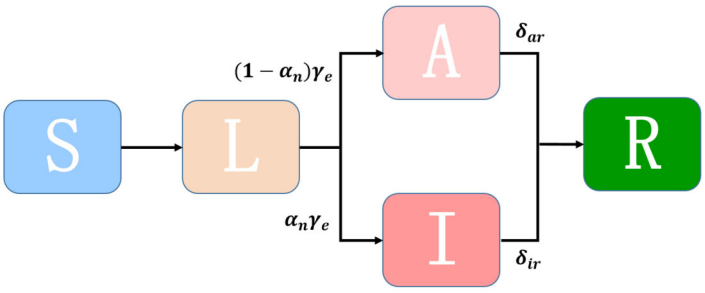

Figure 4 The SLAIR compartmental model structure used in Stages I, II and III

$g(\rho)$.

$$\rho = \frac{\int_0^t \sum_n I_n(\tau)d\tau}{\sum_n \mathcal{N}_n(0)} \tag{4}$$

The function $g(\rho)$ is used to adjust the transmission rate β in the compartmental model. The adjusted transmission rate β' is calculated as $\beta' = \beta \times g(\rho)$, where $g(\rho)$ captures the influence of the attack rate on the transmission rate. In the subsequent sections, we use the adjustment function $g(\rho)$, and taking into account the characteristics of epidemic development at different stages, construct compartmental models.

2.3.2 Stage I pre-opening

Based on the natural history of Omicron, we establish an SLAIR model (Figure 4) to simulate the transmission of SARS-CoV-2 in Shenzhen. This model structure is used in Stages I–III. The dynamic equations of the model are shown in Equation (5). In this model, the population of Shenzhen is divided into four age groups: 0–3, 4–17, 18–59, and 60+ years. The age proportions of each group are derived from the 7th national census data. This model uses an age-specific contact matrix to describe the contact patterns among different sub-populations. The model parameters are shown in Table 1.

$$\begin{cases} \frac{dS_n(t)}{dt} = -\beta_1 g(\rho) S_n(t) \sum_m \left(M_{nm} \frac{A_m(t)+I_m(t)}{N_m} \right) \\ \frac{dL_n(t)}{dt} = \beta_1 g(\rho) S_n(t) \sum_m \left(M_{nm} \frac{A_m(t)+I_m(t)}{N_m} \right) - \gamma_e L_n(t) \\ \frac{dA_n(t)}{dt} = (1-\alpha_n)\,\gamma_e L_n(t) - \delta_{ar} A_n(t) \\ \frac{dI_n(t)}{dt} = \alpha_n \gamma_e L_n(t) - \delta_{ir} I_n(t) \\ \frac{dR_n(t)}{dt} = \delta_{ar} A_n(t) + \delta_{ir} I_n(t) \\ N_n = S_n(t) + L_n(t) + A_n(t) + I_n(t) + R_n(t) \end{cases} \tag{5}$$

- $S_n(t)$, $L_n(t)$, $A_n(t)$, $I_n(t)$ and $R_n(t)$ are the numbers of susceptible, latent, asymptomatic, symptomatic and removed individuals in age group n at time t, respectively.
- N_n represents the total population of age group n.
- M_{nm} represents the average number of daily contacts between individuals in age group n and age group m [46].
- $g(\rho)$ represents the influence of the attack rate on the transmission rate β_1.

Due to the influence of policy changes and human activities, the transmission rate of Omicron varies across different stages. To account for this, the transmission rate β_1 is

Table 1 Model parameters for the four stages

Stage	Parameter	Description	Value	Reference
I	β_1	Transmission rate in Stage I	0.057 (95% CI: 0.055–0.058)	Estimated
I–IV	$1/\gamma_e$	Latent period	$\Gamma(3, 0.1)$ days	[43]
I–IV	α_n	Symptomatic rate by age group	[0.78, 0.75, 0.85, 0.87]	[44]
I–IV	$1/\delta_{ar}$	Infectious period for asymptomatic infections	$\Gamma(8.87, 0.1)$ days	[45]
I–IV	$1/\delta_{ir}$	Infectious period for symptomatic infections	$\Gamma(8.87, 0.1)$ days	[45]
II	β_2	Transmission rate in Stage II	0.090 (95% CI: 0.088–0.091)	Estimated
III-IV	γ, μ	Scaling factor and weight parameter of transmission rate function $\beta(\gamma, \mu)$ in Stages III, IV	0.098 (95% CI: 0.097–0.098), 0.833 (95% CI: 0.832–0.833)	Estimated
IV	$\varphi, \varepsilon, \lambda$	Constituent parameters of the individual immunity waning function $F(\varphi, \varepsilon, \lambda)$	0.036 (95% CI: 0.032–0.036), 0.100 (95% CI: 0.089–0.113), 0.160 (95% CI: 0.151–0.183)	Estimated
IV	$1/\gamma_{rs}$	The period from R (Removed) moving to S′ (Secondary susceptible)	248 (95% CI: 247.5–248.0) days	Estimated

estimated by fitting the SLAIR model to epidemic surveillance data. Specifically, we fit the model to the daily new positive cases calculated based on nucleic acid test data from November 10 to November 31, 2022 in Shenzhen, with β_1 set as the optimization parameter. The mean squared error (MSE) between the simulated daily new infections and the actual nucleic acid test data is used as the objective function, as shown in Equation (6):

$$\operatorname{argmin} f_1(\beta_1) = \frac{1}{n}\sum_{t=1}^{n}\left(L_{\text{model}}(t, \beta_1) - L_{\text{real}}(t)\right)^2, \tag{6}$$

where $L_{\text{model}}(t, \beta_1)$ represents the number of new infections simulated by the model on day t, and $L_{\text{real}}(t, \beta_1)$ represents the actual number of positive nucleic acid tests on day t. The optimal β_1 is determined by the Bayesian optimization algorithm [47]. The Bayesian optimization algorithm is also used in the subsequent stages to estimate unknown parameters.

2.3.3 Stage II relaxation

During this period, despite the relaxation of control policies, human activity levels did not return to pre-pandemic levels, and the scale of infections remained relatively low. The SLAIR model from Stage I is retained in this phase. However, due to policy changes and the resulting shifts in human behavior, the transmission rate changes. Therefore, it is necessary to refit β_2. The positive cases on November 30, 2022, obtained from the simulation in Stage I, are used as the seed for Stage II. We use daily new positive cases calculated based on nucleic acid test data from December 1 to December 6, 2022, to refit β_2. The fitting process in Stage II is mirrors that of Stage I, and the optimal β_2 is again determined using the Bayesian optimization algorithm.

2.3.4 Stage III first wave

Stage III is characterized by an "opening up" after policy adjustments, resulting in significant changes in human mobility compared to earlier stages. These behavioral changes have a considerable impact on contact patterns and the spread of Omicron. Therefore, in this stage, we use population mobility monitoring data as a probe to dynamically adjust the transmission rate, β, from Stages I and II.

We adopt the method proposed by Leung et al. [39] to construct the transmission rate $\beta(t)$, accounting for both population exposure from outdoor activities and household contacts. Specifically, we use intra-urban mobility data from residents of Shenzhen to represent the contact intensity associated with population engagement in outdoor activities. Given the geographical proximity of Shenzhen to Hong Kong, we apply the household contact matrix developed by Leung et al. for Hong Kong [39] to Shenzhen. The transmission rate $\beta(t)$ is calculated as follows:

$$\beta(t) = \mu\gamma m^2(t) + (1-\mu)H. \tag{7}$$

We define $m(t)$ as the normalized intra-urban residential mobility in Shenzhen (https://qianxi.baidu.com) on day t. H represents the average number of contacts within a household, while γ and μ denote the scaling factor and weight parameter, respectively, both of which are estimated through statistical inference. The dynamic equations for the model in Stage III are as follows:

$$\begin{cases} \frac{dS_n(t)}{dt} = -\beta(t)g(\rho)S_n(t)\sum_m \left(M_{nm}\frac{A_m(t)+I_m(t)}{N_m}\right) \\ \frac{dL_n(t)}{dt} = \beta(t)g(\rho)S_n(t)\sum_m \left(M_{nm}\frac{A_m(t)+I_m(t)}{N_m}\right) - \gamma_e L_n(t) \\ \frac{dA_n(t)}{dt} = (1-\alpha_n)\,\gamma_e L_n(t) - \delta_{ar}A_n(t) \\ \frac{dI_n(t)}{dt} = \alpha_n\gamma_e L_n(t) - \delta_{ir}I_n(t) \\ \frac{dR_n(t)}{dt} = \delta_{ar}A_n(t) + \delta_{ir}I_n(t) \\ N_n = S_n(t) + L_n(t) + A_n(t) + I_n(t) + R_n(t). \end{cases} \tag{8}$$

For the Stage III model, we need to infer the unknown parameters γ and μ. The initial seed for the model is the number of individuals in compartments A and I by age group on December 6, 2022, simulated by the Stage II model. We then fit the model parameters by utilizing the peak time (December 27, 2022) of wastewater surveillance data in Shenzhen from December 7, 2022, to January 31, 2023. The objective function is defined as follows:

$$\operatorname{argmin} f_2(\gamma,\mu) = \left|P_{\text{model}}(\gamma,\mu) - P_{\text{real}}\right|, \tag{9}$$

where P_{model} denotes the peak infection time as simulated by the model, where P_{real} is the peak time of infections derived from wastewater surveillance data. Then, the optimal parameters γ and μ are found using the Bayesian optimization algorithm.

2.3.5 Stage IV second wave

After the first Omicron wave in Shenzhen, a natural immunity barrier was established within the population. According to the report of China CDC, the XBB variant became the dominant strain during this stage (https://www.chinacdc.cn). Variants like XBB, along with BA.5/BF.7, belong to the same lineage. While it is known that XBB has greater immune evasion capabilities than BA.5/BF.7 [48], concrete data comparing their transmissibility is lacking. Therefore, in Stage IV, we continue to use the transmission parameter $\beta(t)$ as fitted in Stage III. Considering the potential for reinfection among previously infected individuals and the subsequent development of immunity, we extend the compartmental model used in Stages I–III. The updated model structure is shown in Figure 5.

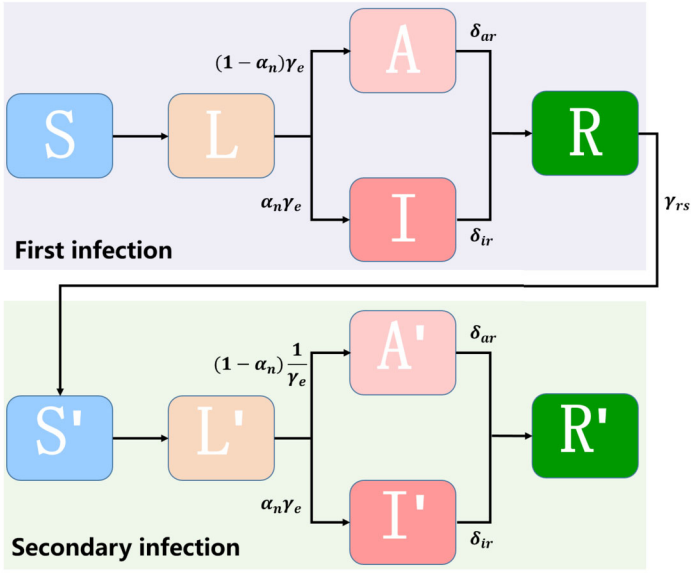

Figure 5 The compartmental model structure for Stage IV

After individuals enter the R compartment, they transition to the S' (secondary susceptible) compartment at a rate γ_{rs}, where they become susceptible to secondary infection. The compartmental transition process for secondary infections mirrors that for primary infection. To reduce the influence of repeated infections on our analysis of secondary infections, we do not account for tertiary infections. In Stage IV, we consider both the immunity conferred by initial infections and its gradual waning over time, which can reduce the risk of reinfection. The process of individual immunity waning is modelled based on prior literature [49], where we assume that the waning function follows a convex-concave shape. We define this function using a sigmoid function. $F(t)$ represents the probability of preventing infection, i.e., the protective ability of prior infection against reinfection.

$$F(t) = \frac{1-\varepsilon}{1+e^{\varphi(t-\lambda)}} + \varepsilon. \tag{10}$$

The unknown parameters are φ, ε, λ. To account for the individual immunity waning, we assume that after individuals enter the R compartment, they transition to the S' compartment at a rate γ_{rs}, making them susceptible to infection again. After determining the individual immunity waning function, we use a weighted average method to calculate population immunity. The calculation formula is as follows:

$$S_{\text{imm}}(t) = \frac{\sum_t S'_{\text{new}}(t)F(t)}{\sum_t S'_{\text{new}}(t)} \tag{11}$$

$S'_{\text{new}}(t)$ represents the number of individuals who became susceptible to secondary infection t days ago, while $S_{\text{imm}}(t)$ represents the average level of population immunity at this

time t.

$$\begin{cases} \frac{dS_n(t)}{dt} = -\beta(t)g(\rho)S_n(t)\sum_m \left(M_{nm}\frac{A_m(t)+I_m(t)+A'_m(t)+I'_m(t)}{N_m}\right) \\ \frac{dL_n(t)}{dt} = \beta(t)g(\rho)S_n(t)\sum_m \left(M_{nm}\frac{A_m(t)+I_m(t)+A'_m(t)+I'_m(t)}{N_m}\right) - \gamma_e L_n(t) \\ \frac{dA_n(t)}{dt} = (1-\alpha_n)\,\gamma_e L_n(t) - \delta_{ar}A_n(t) \\ \frac{dI_n(t)}{dt} = \alpha_n\gamma_e L_n(t) - \delta_{ir}I_n(t) \\ \frac{dR_n(t)}{dt} = \delta_{ar}A_n(t) + \delta_{ir}I_n(t) - \gamma_{rs}R_n(t) \\ \frac{dS'_n(t)}{dt} = \gamma_{rs}R_n(t) - \beta(t)g(\rho)S_{\text{imm}}(t)S'_n(t)\sum_m \left(M_{nm}\frac{A_m(t)+I_m(t)+A'_m(t)+I'_m(t)}{N_m}\right) \\ \frac{dL'_n(t)}{dt} = \beta(t)g(\rho)S_{\text{imm}}(t)S'_n(t)\sum_m \left(M_{nm}\frac{A_m(t)+I_m(t)+A'_m(t)+I'_m(t)}{N_m}\right) - \gamma_e L'_n(t) \\ \frac{dA'_n(t)}{dt} = (1-\alpha_n)\,S_{\text{imm}}(t)\gamma_e L'_n(t) - \delta_{ar}A'_n(t) \\ \frac{dI'_n(t)}{dt} = \alpha_n S_{\text{imm}}(t)\gamma_e L'_n(t) - \delta_{ir}I'_n(t) \\ \frac{dR'_n(t)}{dt} = \delta_{ar}A'_n(t) + \delta_{ir}I'_n(t) \\ N_n = S_n(t) + L_n(t) + A_n(t) + I_n(t) + R_n(t) + S'_n(t) + L'_n(t) + A'_n(t) + I'_n(t) + R'_n(t) \end{cases} \tag{12}$$

We then utilize the peak time of daily reported COVID-19 cases from medical institutions from May 1 to June 2, 2023, along with the trends in the daily case number curve, to fit the unknown model parameters. Specifically, we use the absolute error in peak time between the reported cases and the model-simulated infections, as well as the Pearson correlation coefficient between the simulated and reported daily cases during this period, as objective functions.

$$\begin{aligned} &\operatorname{argmin} f_3(\varphi, \varepsilon, \lambda, \gamma_{rs}) \\ &= \omega_1 |P_{\text{model}} - P_{\text{real}}| + \omega_2 \frac{\sum_t \left(L_{\text{sim}}(t) - \bar{L}_{\text{sim}}\right)\left(L_{\text{real}}(t) - \bar{L}_{\text{real}}\right)}{\sqrt{\sum_t \left(L_{\text{sim}}(t) - \bar{L}_{\text{sim}}\right)^2 \sum_t \left(L_{\text{real}}(t) - \bar{L}_{\text{real}}\right)^2}}, \end{aligned} \tag{13}$$

where P_{model} denotes the simulated peak time of daily new infections in Shenzhen's second Omicron wave, and P_{real} represents the actual peak time of daily reported cases in Shenzhen. $L_{\text{sim}}(t)$ represents the modeled daily new infections from May 1 to June 2, 2023, while $L_{\text{real}}(t)$ represents the daily reported case numbers. ω_1 and ω_2 are weighting coefficients. Finally, the Bayesian optimization algorithm is applied to search for the optimal parameter set that minimizes the value of the objective function.

3 Results

3.1 Model fitting and validation

This section presents the fitting results between the model simulations and real data for each of the four stages.

As shown in Figure 6(a)–(b), the estimated daily COVID-19 cases based on positive rate of nucleic acid testing increased from 10 to 350 during the 20 days of Stage I (November 11–30, 2022), and surged to 1,966 over the 6 days of stage II (December 1–6, 2022). In Figure 6(c)–(d), the model simulation of daily new infections fits the number of positive cases quite well in both stages, with Pearson correlation coefficients of 0.96 and 0.98, respectively. These models are used to capture the scale of infection seeds at the beginning of the first Omicron wave.

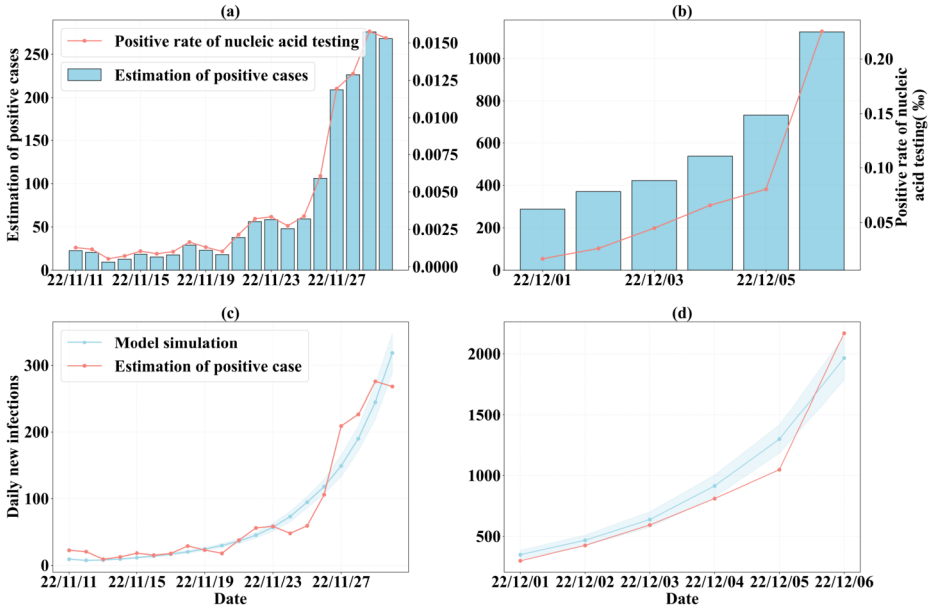

Figure 6 The model simulations of daily new infections according to the reported positive rate of nucleic acid testing in Stages I and II. (a) Positive rate of nucleic acid testing in Stage I (November 11 – November 30, 2022). (b) Positive rate of nucleic acid testing in Stage II (December 1–6, 2022). (c) Model simulation of daily new infections in Stage I. (d) Model simulation of daily new infections in Stage II

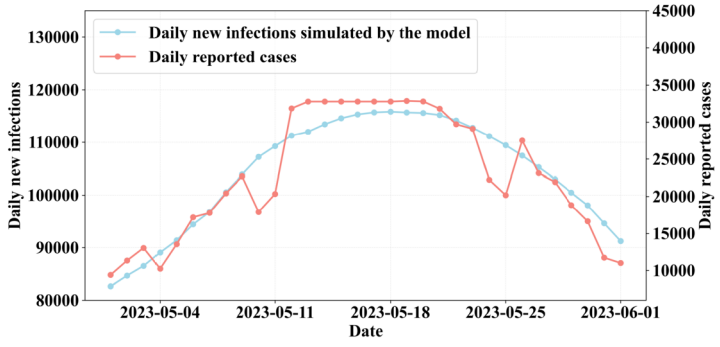

Figure 7 The model fitting results in Stage IV

In Stage III (the first Omicron wave), the model is fitted using the peak infection time derived from wastewater surveillance data, with the peak occurring on December 27, 2022. As shown in Figure 8(a), the modeled peak time aligns well the observed peak on December 27.

In Stage IV (the second Omicron wave), we fit the model using the full trend of daily reported cases from May 1 to June 2, 2023, as shown in Figure 7. Due to the prevalence of mild symptoms during this wave in Shenzhen, a substantial discrepancy exists between the daily reported cases and the actual daily new infections. Therefore, the model fitting focuses on the peak time and the overall trend of the reported case curve. As a result, both the simulated and reported daily new infections peaked on May 18, 2023, with a Pearson correlation coefficient of 0.93 between the two curves.

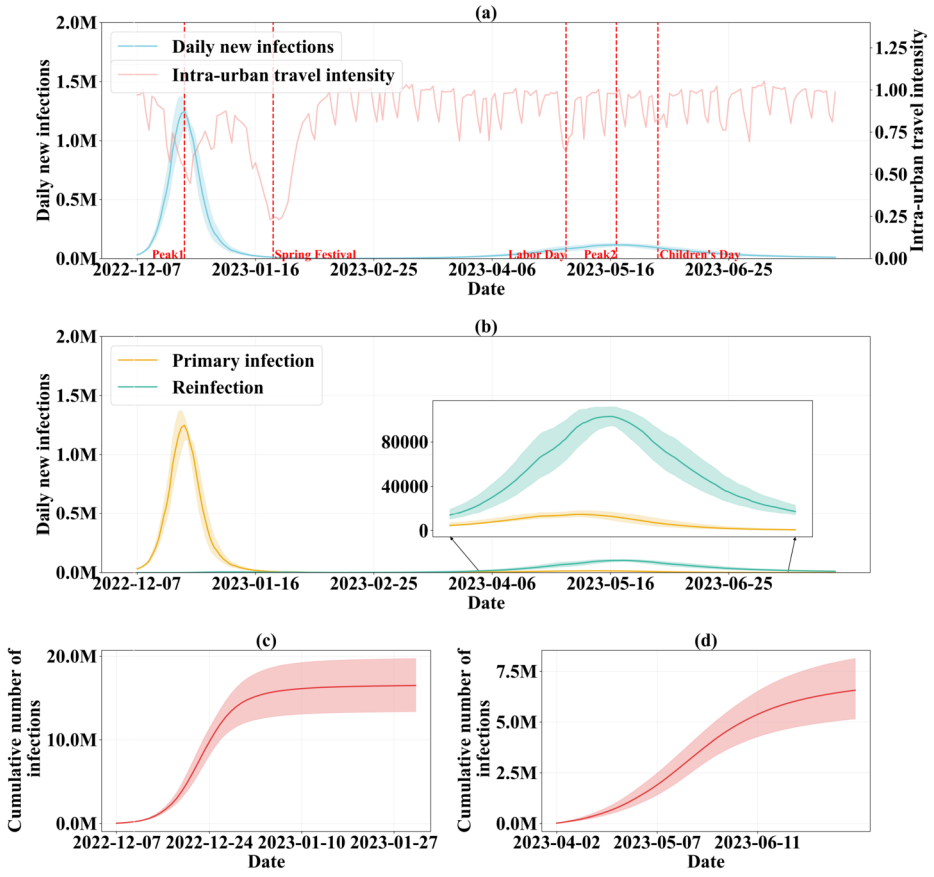

Figure 8 The modeled two consecutive waves of Omicron in Shenzhen. (a) Daily new infections during the two consecutive waves. (b) Daily new infections segmented by primary infections and reinfections. (c) Cumulative infections during the first Omicron wave. (d) Cumulative infections during the second Omicron wave

3.2 The first Omicron wave in Shenzhen

This section delves into the details of the first Omicron wave in Shenzhen and the changes in human mobility.

Figure 8(a) displays the daily new infections in Shenzhen. The peak of the first Omicron wave occurred on December 23, 2022 (Peak 1), with an estimated peak value of approximately 1.25 million (95% CI: 1.11–1.32 million) and a peak daily new infection rate of 7.13% (95% CI: 6.36-7.53%). By January 3, 2023, the daily new infection rate had dropped to below 1%, and the attack rate for the first wave in Shenzhen reached 88.5% (95% CI: 72.1–99.6%).

In Figure 8(a), from December 7 to December 23, 2022, daily new infections in Shenzhen experienced rapid growth. During this period, the travel intensity in Shenzhen dropped significantly, reaching 0.44 on December 25, 2022 — two days after the infection peak- which represents a decrease of approximately 56% compared to normal travel intensity. The two-day lag in mobility decrease is likely due to the 2-3 day incubation period. Given the high percentage of symptomatic cases [36], many sick people had to stay at home, and their household members may need to take care of them, leading to a significant decrease in mobility. As the epidemic subsided, travel behavior gradually recovered. More-

over, from January 11 to January 31, 2023, marked the Chinese New Year period–Spring Festival holidays. Shenzhen is China's youngest city, comprising a large number of young workers from other regions, with 63% non-registered residents. Therefore, during the holidays for family reunion, Shenzhen experienced significant population outflow, resulting in the lowest point of intra-urban travel intensity. At the same time, the first Omicron wave in Shenzhen has ended, so it did not significantly impact the epidemic.

3.3 The second Omicron wave in Shenzhen

We define the beginning of the second Omicron wave as the date when the daily new infections exceed 0.1% after the conclusion of the first Omicron wave, and consider it over when the daily new infections drop again below 0.1%. According to the model simulation, the second Omicron wave in Shenzhen started on April 2, 2023, and ended on July 15, 2023, peaking on May 18, 2023 (Peak 2). At its peak, the daily new infections reached 0.12 million (95% CI: 0.10–0.13 million), corresponding to a new infection rate of 0.66% (95% CI: 0.59– 0.73%). As shown in Figure 8(d), the cumulative number of infections during the second wave was 6.57 million (95% CI: 5.16–8.14 million), with an attack rate of 37.5% (95% CI: 29.5–46.4%). Figure 8(b) illustrates the daily new infections segmented by primary infections and reinfections across both waves. During the first Omicron wave, the majority of daily new infections were primary. Following the conclusion of the first wave, the daily primary infections gradually decreased, while reinfections started to rise. On February 23, 2023, the daily new reinfections surpassed primary infections. During the second wave, reinfections become predominant. On May 18, 2023, at the peak of the second wave, the daily new primary infections were 13 k (95% CI: 10–16k), while reinfections reached 0.102 million (95% CI: 0.09–0.11million). The attack rate for primary infections in the second wave was 4.2% (95% CI: 3.2–5.6%), while the attack rate for reinfections was 33.3% (95% CI: 26.3–40.8%), accounting for 88.8% of infections during the second wave.

As observed in Figure 8(a), after the Chinese New Year, intra-urban travel intensity in Shenzhen returned to normal levels and exhibited a weekly rhythmic pattern. During the second Omicron wave, there was no significant change in intra-urban mobility in Shenzhen. Cross-correlation function analysis indicates a very strong negative correlation (coefficient = −0.98, $P = 0.0035$) at lag 0 between the number of new infections in the first wave and travel intensity, suggesting that a decrease in mobility was closely associated with an increase in new infections and vice versa. In contrast, the correlation between the second wave and travel intensity was much weaker (coefficient = −0.25, $P = 0.3$), suggesting a less pronounced relationship. Thus, it can be inferred that the second Omicron wave had a limited impact on the daily travel behavior of Shenzhen residents.

3.4 Immunity and immune waning

During the first Omicron wave in Shenzhen, the predominant strain was BA.5/BF.7. The XBB variant was first detected in China on February 17, 2023, and subsequently became the dominant strain in the second wave (https://www.chinacdc.cn). Individuals previously infected with the BA.5/BF.7 subvariants may develop partial immunity to the XBB subvariant, providing some protection against reinfection. However, this immunity wanes over time. To model this process, we fit the dynamics of individual immunity and its decline (see Figure 11). In our model, individuals gain immunity against Omicron reinfection after an initial infection. We present the simulation results as an alternative to a closed cohort

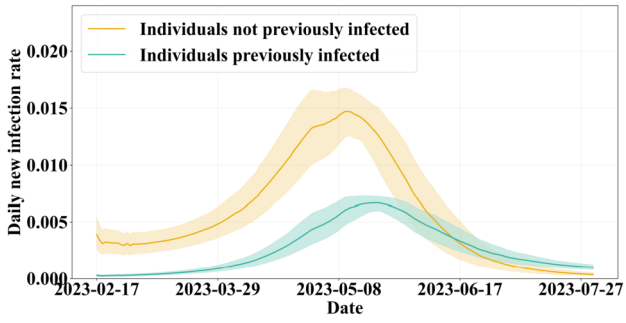

Figure 9 The daily new infection rate for the control group and the test group

to assess the protective effect against XBB reinfection after infection with BA.5/BF.7. The observation time spanned from February 17 to July 31, 2023. As shown in Figure 9, the orange line represents the daily new infection rate in the simulated control group, which had no prior SARS-CoV-2 infection before XBB infection, while the green line represents the simulated test group, previously infected with BA.5/BF.7 subvariants. The control group peaked on May 11, 2023, whereas the test group peaked nine days later on May 20, 2020, with about 45% of the daily new infection rate of the control group. The relative risk (RR), defined as the ratio of the attack rate among previously infected individuals to that of those without prior infection, was calculated to be 0.451 (95% CI: 0.448-0.456). This suggests a 0.549 (95% CI: 0.544-0.552) protective effect against XBB reinfection after previous infection with BA.5/BF.7 subvariants within 6 months.

3.5 Comparison of epidemic characteristics between the two consecutive Omicron waves in Shenzhen

The instantaneous effective reproduction number, R_t, is defined as the average number of secondary cases per infectious case on day t. We used the "EpiEstim" R package developed by Thompson et al. [50] to calculate the R_t values for the two consecutive Omicron waves. As shown in Figure 10, just on December 11, 2022 – shortly after opening up – R_t reached 5.44. Following this, due to the rapid and dramatic increase of symptomatic patients (especially with fever [44]), and the need to care for household members, out-of-home travels have dropped dramatically throughout the city. On December 25, 2022, symptomatic cases in Shenzhen reached their peak, and intra-urban travel intensity fell to its lowest point of 0.44, while R_t decreased to 1.36 (95% CI: 1.32-1.37). After the wave passed its peak, cases gradually recovered and the intra-urban travel intensity gradually increased. R_t dropped below 1 on December 27, 2022. During the Spring Festival, Shenzhen experienced a large-scale population outflow, which further reduced the intra-urban travel intensity to its lowest point of 0.23. By that time, the first Omicron wave in Shenzhen had basically ended, with R_t fluctuating around 0.6. At the beginning of the second wave, R_t was 1.28 (95% CI: 1.27-1.29), and remained stable for about a month, falling below 1 for the first time on May 22, 2023. Throughout the second wave, R_t remained low (0.85-1.3), and the intra-urban travel intensity maintained normal levels, indicating that the daily mobility in Shenzhen was not greatly affected during the second wave.

As shown in Table 2, the duration of the second wave was approximately three times longer than the first. The peak times of the two waves were five months apart. The first

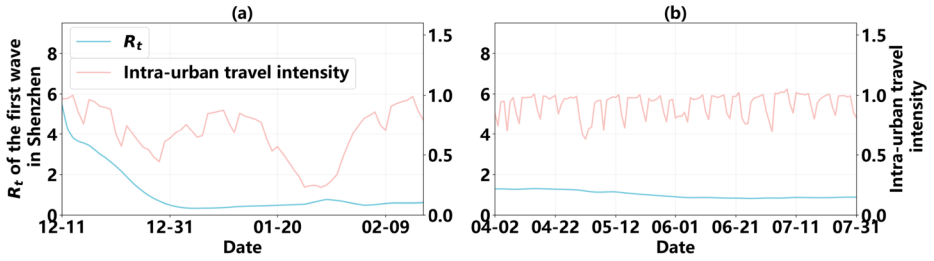

Figure 10 R_t of the two consecutive Omicron waves in Shenzhen after opening up

Table 2 Comparison of the epidemic characteristics of the first and second Omicron waves

	Start	End	Duration	Peak time	Peak daily new infections	Attack rate
First wave	12/07/2022	01/03/2023	28 days	12/23/2022	1.25 m	88.5%
Second wave	04/02/2023	07/15/2023	104 days	05/18/2023	0.12 m	37.5%

wave reached its peak in 16 days, while the second wave took 47 days to do so - about three times longer. The peak daily new infections in the second wave was roughly one-tenth of those in the first, with an attack rate about two-fifths that of the first wave.

4 Discussion and conclusions

In large-scale epidemics, relying solely on a single data source and a compartmental model makes it difficult to quickly and accurately assess epidemic dynamics. To overcome this limitation, this study develops an epidemic modeling framework that integrates multi-source data. To address the issue of overestimating attack rates in the compartmental model, we introduce an ABM to increase heterogeneity. This hybrid modeling framework provides a valuable approach to accurately assess epidemic spread in urban environments using multi-source surveillance data.

Our simulations estimate the attack rate of the first Omicron wave in Shenzhen to be 88.5%, which is lower than the 97% reported by a previous study [26], based primarily on an online infection status survey conducted on December 26, 2022. Online surveys can overestimate infection rates for several reasons: 1) Internet users tend to be younger and have higher contact rates with fewer protective behaviors, leading to higher infection rates; 2) Individuals who are infected and symptomatic are more likely to participate in such surveys. In contrast, our estimate aligns closely with the results from more reliable sources. For instance, a serological survey in Guangzhou, another megacity in the same province located 100 kilometers from Shenzhen, reported an IgM+ rate of 87% [36], supporting the accuracy of our model. Additionally, Fu et al. [51] estimated a national attack rate of the first wave to be 82.4% based on an online survey. We infer that Shenzhen, as the youngest city in China with potentially more human contacts, experienced a higher attack rate compared to the national average.

When examining secondary infections in the population, we account for both high immune escape and the process of immune waning. Model simulations estimate that there is only 54.9% protective effect against XBB reinfection within 6 months after a first infection of BA.5/BF.7. A retrospective cohort study in Singapore also reported that immunity against XBB infection remains high 7-8 months after infection with the Omicron BA.2,

BA.5 and BF.7 variants [38]. According to results from a UK cohort study, the risk of reinfection with XBB after an initial infection with BA.5/BF.7 variants increased from 0.5 to 1 over approximately 120 days, with a reinfection rate of 14-16% for XBB identified. Comparing these results with other countries, we observed a faster decay in population immunity and a higher reinfection rate of 33.3% in our population. This is likely attributed to the unique policy decisions in China, as other countries have experienced multiple epidemic waves, allowing their populations to accumulate immunity against various strains. In contrast, China's consecutive waves occurred when a majority of the population lack natural immunity to SARS-CoV-2. Whether the new variant causes a spike in the number of infections in a given country is likely to depend on the size and timing of that country's earlier wave, as noted by an evolutionary biologist from the Catholic University of Leuven in Belgium [52]. Wu et al. [29] and Wang et al. [14] projected that mainland China would face its second wave 7 months after the first, with an attack rate of about 37%, based on assumptions of antibody efficacy. We fill in their assumptions with our fitted results based on real surveillance data, further validating their projection about the infection rate of the second wave. We found that the actual peak time in Shenzhen and mainland China occurred in May 2023 (https://www.chinacdc.cn), which is 2-3 months earlier than predicted by models based on assumptions.

During the initial phase of the first Omicron wave, despite the absence of travel restrictions, mobility significantly decreased. This reduction can be attributed to the rapid spread of the epidemic, potentially leading to numerous concentrated infections, particularly among those with fever, which reduced the movement of both patients and their caregivers. Additionally, some individuals voluntarily self-isolated, and fear-driven preventive behaviors further contributed to reduced mobility [25]. In contrast, the second wave had a less noticeable impact on mobility. The scale of infections was significantly lower, symptoms during reinfections were milder, and increased public awareness and understanding of COVID-19 diminished fear. As a result, population mobility remained stable. When substantial changes in mobility occur, it is essential for models to incorporate these variations in contact patterns to accurately simulate epidemic dynamics.

In summary, our study demonstrates that for a completely susceptible population, two consecutive Omicron waves are likely to result in widespread infection. However, due to the rapid mutation of SARS-CoV-2, the swift waning of immunity, and the absence of seasonality, reinfection remains a concern. Therefore, real-time surveillance of infection rates, severe cases, and mortality remains crucial.

This study has several limitations. First, the immune waning mechanism in our model does not account for age-specific differences. In reality, immune response and the rate of waning vary by age due to physiological factors, resulting in heterogeneity [53]. Second, due to the unavailability of local social contact data, we used the age-specific contact matrix from Hong Kong as a proxy for Shenzhen. Given the demographic and social similarities between Hong Kong and Shenzhen — such as urban settings, population density, and cultural practices — this substitution is unlikely to significantly affect our conclusions.

Appendix

A.1 Synthetic population

This section refers to the method by Zhu et al. (2024) [42]. To simulate disease transmission within a city, we first constructed a synthetic population that reflects the actual

demographics of the target city. This process used census data and household survey data to generate a synthetic population that matches the scale and demographic characteristics of the real urban population. We used combinatorial optimization to align key demographic attributes, such as age distribution and household size, while preserving typical family structures to ensure consistency with statistical data. Specifically, we derived typical household structures from survey data and applied combinatorial optimization to match the marginal distributions of key attributes (e.g., age, household size) based on census data. This optimization involved heuristic constraint techniques to produce an optimal allocation scheme, ensuring high consistency between the synthetic population and actual demographic distributions.

A.2 Contact network construction

This section refers to the work by Yin et al. (2021) [41]. To accurately represent the contact network characteristics, we constructed a multi-level contact network based on individuals' location and behavior attributes from the synthetic population. Real-world contact networks consist of both fixed contacts, based on social relationships, and dynamic contacts, based on spatial proximity. Thus, we categorized the contact network into four types: Household, Workplace, School, and Community. Each network type was assigned different contact mechanisms and intensities.

Data usage:

- Census data (including population age structure and household size distribution): used to construct a synthetic population with accurate age structure and household size distribution.
- Household structure survey data: employed to further refine household composition in the synthetic population, aligning with the typical household structure in the target city.
- Employment rate data: utilized to determine parameters for the workplace network, helping to identify employed individuals and set their workplace locations.
- Contact survey data and time-use data: applied to define contact weight parameters across network layers, reflecting individual-level heterogeneity and age-specific contact distributions.

For the Workplace network, we grouped synthetic individuals by their workplace locations, simulating environments such as office buildings or factories. These individuals were then further divided into social groups representing smaller, high-contact groups (e.g., departments or teams) within each workplace, forming a high-frequency contact network. Similarly, school-age individuals were assigned to schools based on educational district data and then subdivided into classrooms, forming the school network. The community network represents individuals' interactions in public spaces, organized randomly at the community level to allow contact opportunities across the population.

Individuals within the same social group (e.g., classrooms or workgroups) have a predetermined set of daily contacts. However, the actual contact count and intensity are determined by parameters based on contact surveys, which define the contact rate (the number of individuals contacted) and contact strength (probability of an infection event per contact). Contact rates across age groups fit a log-normal distribution, highlighting a small number of "hub" individuals with high contact degrees. Overall, students have the highest contact rates, while the elderly have the lowest; Household networks have the highest contact intensity, while Community networks have the lowest.

Table 3 Person-to-person contact intensity within various contact settings. *Sourced from Yin et al. (2021) [41]

Contact setting	Contact intensity	
Home		0.37
Community place	Kindergarten	0.25
	School (elementary, middle, and high)	0.25
	Workplace	0.26
Public place		0.10

We use the predefined weight wk, which reflects the relative importance of contact time in each layer based on survey and time-use data. This data provided records of person-to-person contact durations across different environments, helping us define contact intensity for each setting, as shown in Table 3.

A.3 Spatiotemporal transmission simulation

To simulate disease transmission, we employed a spatially explicit agent-based model that operates in daily discrete iterations. The model initializes with a few infected seed agents, following which each iteration consists of two main processes:

- Contact Infection: Each day, the model scans infectious individuals and simulates contact interactions in different settings using the multi-level contact network. Infectious individuals probabilistically infect susceptible contacts based on their location and contact network type.
- Compartmental Transition: For all non-susceptible individuals, the model simulates changes in their compartmental state over time. The duration in each compartment follows a log-normal distribution to reflect real-world tail characteristics. For compartments with multiple possible outcomes (e.g., severe cases might recover or result in death), we applied a stochastic chain binomial process to ensure random outcomes.

A.4 Individual immunity waning

The immunity process consists of two parts: high immunity and immune waning. After an initial infection, individuals recover and enter the R (Removed) compartment, where they have high protection against reinfection. The parameter $1/\gamma_{rs}$ represents the average duration it takes for an individual to move from the R to the S' (secondary susceptible) compartment, following an exponential distribution with γ_{rs} as the mean. By fitting the Stage IV model, we estimate $1/\gamma_{rs} = 248$ days. Figure 11(a) shows the daily probability of an individual transition from the R back to the S' compartment. On average, the probability is 1/248 per day, and increases over time. By day 170, the probability of transition reaches 0.5. Once in the S' compartment, individuals face a reduced risk of reinfection due to immunity, but this immunity wanes over time. The pattern of individual immune waning is depicted in Figure 11(b), showing a concave-convex curve. In the first 87 days, probability of preventing reinfection declines rapidly to 0.34, after which the decline slows, eventually stabilizing at 0.1.

A.5 Sensitivity analysis on household contacts

In our study, contact matrices are categorized into household and external household contact matrices. The external household contact matrix is based on data from Shenzhen,

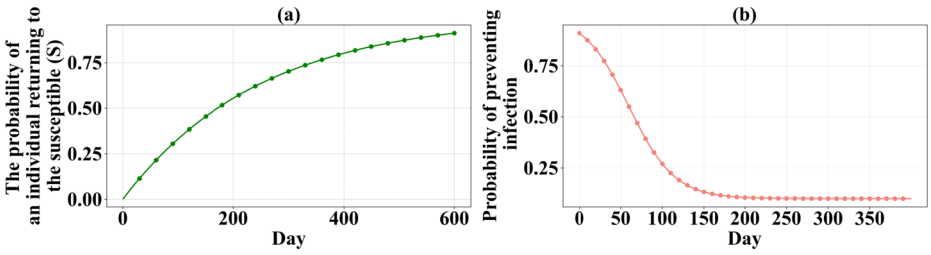

Figure 11 The individual immunity and immune waning function of infection with BA.5/BF.7 against XBB reinfection. (a) The probability of an individual returning to the susceptible. (b) The individual immune waning function of infection with BA.5/BF.7 against XBB reinfection

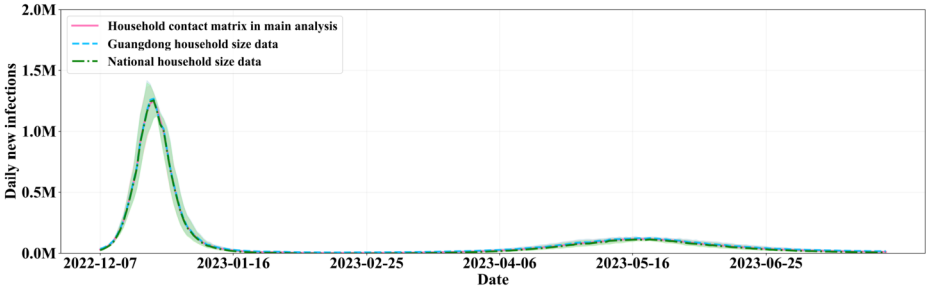

Figure 12 Daily new infections based on different household contact intensities

while, due to the lack of specific household contact data for Shenzhen, we use the household contact matrix from Hong Kong. From this matrix, we derive the average household contact intensity. To assess the impact of using this contact matrix on the experimental outcomes, we conduct a sensitivity analysis. The average household sizes for the country and Guangdong province are obtained from the 7th National Population Census and a social survey [54], respectively. We use these household sizes as a rough proxy for household contact intensity in Guangdong and nationwide, and refit the model for Stages III and IV. The fitted daily new infections are shown in Figure 12. The peak of the first wave, using the household contact matrix in the main text, is 1.247 m, whereas the values for Guangdong and nationwide data are 1.262 m and 1.259 m, respectively, showing minimal differences. The peak of the second wave under the contact matrix in the main text is 0.115 m, compared to 0.121 m (Guangdong) and 0.123 m (nationwide), also indicating small variations. The cumulative infection rate of the first wave is almost identical across the three data sets, at 0.885, 0.886, and 0.889, respectively. Similarly, the cumulative infection rates for the second wave are 37.5% (contact matrix in the main text), 37.7% (Guangdong), and 38.2% (nationwide). In conclusion, given the similarity in average household sizes between Guangdong and nationwide data, the household contact intensities also exhibit little variation. The model fitting results for both waves indicate that the differences across the three data sets are minimal, with limited impact on the overall findings.

Author contributions

YS, LY, KZ, ZZ and QL conceived the idea, designed the study, analyzed the data, and prepared a draft of the manuscript. JC and KL contributed to the methodological design and actively participated in conducting a critical review of the manuscript. DK and ZC participated in data collection. All authors critically reviewed the content of the manuscript for methodological validity and sound interpretation of the findings and agreed to submit it for publication. All authors read and approved the final manuscript.

Funding
This work was supported by the National Natural Science Foundation of China (No.42271475), the Basic and Applied Basic Research Foundation of Guangdong Province (2022B1515120064), the Key Project of Shenzhen Science and Technology Innovation Commission (JCYJ202103241154-11030), Shenzhen Key Medical Discipline Construction Fund (SZXK064), Shenzhen San-Ming Project of Medicine in Shenzhen (SZSM202011008), and Shenzhen Municipal Technological Project (JCYJ20200109150715644).

Data availability
Shenzhen demographic data and intra-urban mobility data are publicly available (https://qianxi.baidu.com; https://www.gov.cn/guoqing/202105/13/content_5606149.htm). For access to epidemic surveillance data in Shenzhen, please contact the following email address: sandylv1980@126.com

Declarations

Competing interests
The authors declare no competing interests.

Author details
[1]Shenzhen Institutes of Advanced Technology, Chinese Academy of Sciences, Shenzhen, China. [2]University of Chinese Academy of Sciences, Beijing 100049, China. [3]Department of Communicable Diseases Control and Prevention, Shenzhen Center for Disease Control and Prevention, Shenzhen 518055, China. [4]School of Public Health, Southern Medical University, Guangzhou 510515, China. [5]School of Public Health, Key Laboratory of Public Health Safety, Ministry of Education, Fudan University, Shanghai, China. [6]Faculty of Computer Science and Control Engineering, Shenzhen University of Advanced Technology, Shenzhen, China.

Received: 23 July 2024 Accepted: 10 December 2024 Published online: 09 January 2025

References

1. Ibrahim, A., Humphries, U.W., Ngiamsunthorn, P.S., Baba, I.A., Qureshi, S., Khan, A.: Modeling the dynamics of COVID-19 with real data from Thailand. Sci. Rep. **13**(1), 13082 (2023)
2. Msemburi, W., Karlinsky, A., Knutson, V., Aleshin-Guendel, S., Chatterji, S., Wakefield, J.: The WHO estimates of excess mortality associated with the COVID-19 pandemic. Nature **613**(7942), 130–137 (2023)
3. Ozili, P.K., Arun, T.: Spillover of COVID-19: impact on the global economy. In: Managing Inflation and Supply Chain Disruptions in the Global Economy, pp. 41–61. IGI Global (2023)
4. Tian, H., Liu, Y., Li, Y., Wu, C.-H., Chen, B., Kraemer, M.U., et al.: An investigation of transmission control measures during the first 50 days of the COVID-19 epidemic in China. Science **368**(6491), 638–642 (2020)
5. Xiao, H., Liu, F., Unger, J.M.: Dynamic zero-COVID policy and healthcare utilization patterns in China during the Shanghai COVID-19 Omicron outbreak. Commun. Med. **3**(1), 143 (2023)
6. Burki, T.: Dynamic zero COVID policy in the fight against COVID. Lancet Respir. Med. **10**(6), e58–e59 (2022)
7. Liu, J., Liu, M., Liang, W.: The dynamic COVID-zero strategy in China. China CDC Weekly **4**(4), 74 (2022)
8. Mallapaty, S.: Can China avoid a wave of deaths if it lifts strict zero COVID policy. Nature **612**(7939), 203 (2022)
9. Xinhua: China Focus: China releases measures to optimize COVID-19 response (2022). [Available from https://english.news.cn/20221111/d4399114a082438eaac32d08a02bf58d/c.html]
10. Xinhua: China Focus: COVID-19 response further optimized with 10 new measures (2022). [Available from https://english.news.cn/20221207/ca014c043bf24728b8dcbc0198565fdf/c.html]
11. Xinhua: Beijing sets up fever clinics in all community health service centers (2022). [Available from https://english.news.cn/20221213/2e070d9abcbd4362b990b7e8811b5642/c.html]
12. Xinhua: Chinese vice premier stresses need to ensure smooth transition of COVID-19 response phases (2022). [Available from https://english.news.cn/20221214/3c1d5934a43d47d4a016194acea7bd1d/c.html]
13. Du, Z., Wang, Y., Bai, Y., Wang, L., Cowling, B.J., Meyers, L.A.: Estimate of COVID-19 deaths 2022–February 2023. Emerg. Infect. Dis. **29**, 2121 (2023)
14. Wang, S.-T., Wu, Y.-P., Li, L., Li, Y., Sun, G.-Q.: Forecast for peak infections in the second wave of the Omicron after the adjustment of zero-COVID policy in the mainland of China. Infect. Dis. Model. (2023)
15. Mathieu, E., Ritchie, H., Rodés-Guirao, L., Appel, C., Giattino, C., Hasell, J., et al.: Coronavirus Pandemic (COVID-19). Our World in Data (2020)
16. Sarkar, A., Chakrabarti, A.K., Dutta, S.: Covid-19 infection in India: a comparative analysis of the second wave with the first wave. Pathogens **10**(9), 1222 (2021)
17. Deng, Y., Zheng, X., Xu, X., Chui, H.-K., Lai, W.-K., Li, S., et al.: Use of sewage surveillance for COVID-19: a large-scale evidence-based program in Hong Kong. Environ. Health Perspect. **130**(5), 057008 (2022)
18. Naughton, C.C., Roman, F.A. Jr, Alvarado, A.G.F., Tariqi, A.Q., Deeming, M.A., Kadonsky, K.F., et al.: Show us the data: global COVID-19 wastewater monitoring efforts, equity, and gaps. FEMS Microbes **4**, xtad003 (2023)
19. Li, Y., Du, C., Lv, Z., Wang, F., Zhou, L., Peng, Y., et al.: Rapid and extensive SARS-CoV-2 Omicron variant infection wave revealed by wastewater surveillance in Shenzhen following the lifting of a strict COVID-19 strategy. Sci. Total Environ. **949**, 175235 (2024)
20. Lau, J.J., Cheng, S.M., Leung, K., Lee, C.K., Hachim, A., Tsang, L.C., et al.: Real-world COVID-19 vaccine effectiveness against the Omicron BA. 2 variant in a SARS-CoV-2 infection-naive population. Nat. Med. **29**(2), 348–357 (2023)
21. Zheng, X., Gong, F., Wei, X., Dong, Y., Chen, R., Tang, C., et al.: Accuracy of serological tests for COVID-19: a systematic review and meta-analysis. Front. Public Health **10**, 923525 (2022)
22. Khairulbahri, M.: The SEIR model incorporating asymptomatic cases, behavioral measures, and lockdowns: lesson learned from the COVID-19 flow in Sweden. Biomed. Signal Process. Control **81**, 104416 (2023)

23. Maged, A., Ahmed, A., Haridy, S., Baker, A.W., Xie, M.: SEIR model to address the impact of face masks amid COVID-19 pandemic. Risk Anal. **43**(1), 129–143 (2023)
24. Xu, C., Yu, Y., Ren, G., Sun, Y., Si, X.: Stability analysis and optimal control of a fractional-order generalized SEIR model for the COVID-19 pandemic. Appl. Math. Comput. **457**, 128210 (2023)
25. Leung, K., Lau, E.H., Wong, C.K., Leung, G.M., Wu, J.T.: Estimating the transmission dynamics of SARS-CoV-2 Omicron BF. 7 in Beijing after adjustment of the zero-COVID policy in November–December 2022. Nat. Med. **29**(3), 579–582 (2023)
26. Goldberg, E.E., Lin, Q., Romero-Severson, E.O., Ke, R.: Swift and extensive Omicron outbreak in China after sudden exit from 'zero-COVID' policy. Nat. Commun. **14**(1), 3888 (2023)
27. Zhang, T., Yang, L., Han, X., Fan, G., Qian, J., Hu, X.: Methods on COVID-19 Epidemic Curve Estimation During Emergency Based on Baidu Search Engine and ILI Traditional Surveillance in Beijing, China. Engineering (2023)
28. Ma, Y., Xu, S., Luo, Y., Peng, J., Guo, J., Dong, A., et al.: Predicting the transmission dynamics of novel coronavirus infection in Shanxi province after the implementation of the "Class B infectious disease Class B management" policy. Front. Public Health **11**, 1322430 (2023)
29. Wu, Y., Zhou, W., Tang, S., Cheke, R.A., Wang, X.: Prediction of the next major outbreak of COVID-19 in Mainland China and a vaccination strategy for it. R. Soc. Open Sci. **10**(8), 230655 (2023)
30. Bansal, S., Grenfell, B.T., Meyers, L.A.: When individual behaviour matters: homogeneous and network models in epidemiology. J. R. Soc. Interface **4**(16), 879–891 (2007)
31. Tkachenko, A.V., Maslov, S., Elbanna, A., Wong, G.N., Weiner, Z.J., Goldenfeld, N.: Time-dependent heterogeneity leads to transient suppression of the COVID-19 epidemic, not herd immunity. Proc. Natl. Acad. Sci. **118**(17), e2015972118 (2021)
32. Wei, J., Stoesser, N., Matthews, P.C., Khera, T., Gethings, O., Diamond, I., et al.: Risk of SARS-CoV-2 reinfection during multiple Omicron variant waves in the UK general population. Nat. Commun. **15**(1), 1008 (2024)
33. Carazo, S., Skowronski, D.M., Brisson, M., Barkati, S., Sauvageau, C., Brousseau, N., et al.: Protection against omicron (B. 1.1. 529) BA. 2 reinfection conferred by primary omicron BA. 1 or pre-omicron SARS-CoV-2 infection among health-care workers with and without mRNA vaccination: a test-negative case-control study. Lancet Infect. Dis. **23**(1), 45–55 (2023)
34. Altarawneh, H.N., Chemaitelly, H., Ayoub, H.H., Hasan, M.R., Coyle, P., Yassine, H.M., et al.: Protective effect of previous SARS-CoV-2 infection against Omicron BA. 4 and BA. 5 subvariants. N. Engl. J. Med. **387**(17), 1620–1622 (2022)
35. Li, Z., Hu, P., Qu, L., Yang, M., Qiu, M., Xie, C., et al.: Molecular epidemiology and population immunity of SARS-CoV-2 in Guangdong (2022–2023) following a pivotal shift in the pandemic. Nat. Commun. **15**(1), 7033 (2024)
36. Huang, J., Zhao, S., Chong, K.C., Zhou, Y., Lu, W., Fang, F., et al.: Infection rate in Guangzhou after easing the zero-COVID policy: seroprevalence results to ORF8 antigen. Lancet Infect. Dis. **23**(4), 403–404 (2023)
37. Zheng, B., Gonçalves, B., Deng, P., Wang, W., Tian, J., Liang, X., et al.: Protection afforded by post-infection SARS-CoV-2 vaccine doses: a cohort study in Shanghai. eLife (2024)
38. Tan, C.Y., Chiew, C.J., Pang, D., Lee, V.J., Ong, B., Lye, D.C., et al.: Protective immunity of SARS-CoV-2 infection and vaccines against medically attended symptomatic omicron BA. 4, BA. 5, and XBB reinfections in Singapore: a national cohort study. Lancet Infect. Dis. (2023)
39. Leung, K., Wu, J.T., Leung, G.M.: Real-time tracking and prediction of COVID-19 infection using digital proxies of population mobility and mixing. Nat. Commun. **12**(1), 1501 (2021)
40. Yang, H., Chen, D., Jiang, Q., Yuan, Z.: High intensities of population movement were associated with high incidence of COVID-19 during the pandemic. Epidemiol. Infect. **148**, e177 (2020)
41. Yin, L., Zhang, H., Li, Y., Liu, K., Chen, T., Luo, W., et al.: A data driven agent-based model that recommends non-pharmaceutical interventions to suppress coronavirus disease 2019 resurgence in megacities. J. R. Soc. Interface **18**(181), 20210112 (2021)
42. Zhu, K., Yin, L., Liu, K., Liu, J., Shi, Y., Li, X., et al.: Generating synthetic population for simulating the spatiotemporal dynamics of epidemics. PLoS Comput. Biol. **20**(2), e1011810 (2024)
43. Song, J.S., Lee, J., Kim, M., Jeong, H.S., Kim, M.S., Kim, S.G., et al.: Serial intervals and household transmission of SARS-CoV-2 Omicron variant, South Korea, 2021. Emerg. Infect. Dis. **28**3, 756 (2022)
44. Liu, R., Zhang, Y., Ma, J., Wang, H., Lan, Y., Tang, X.: Epidemiological features of SARS-CoV-2 Omicron infection under new control strategy: a cross-sectional study of the outbreak since December 2022 in Sichuan, China. BMC Public Health **23**(1), 1–12 (2023)
45. Hay, J.A., Kissler, S.M., Fauver, J.R., Mack, C., Tai, C.G., Samant, R.M., et al.: Quantifying the impact of immune history and variant on SARS-CoV-2 viral kinetics and infection rebound: a retrospective cohort study. eLife **11**, e81849 (2022)
46. Mistry, D., Litvinova, M., Pastore y Piontti, A., Chinazzi, M., Fumanelli, L., Gomes, M.F.C., Haque, S.A., et al.: Inferring high-resolution human mixing patterns for disease modeling. Nat. Commun. **12**(1), 323 (2021)
47. Wang, X., Jin, Y., Schmitt, S., Olhofer, M.: Recent advances in Bayesian optimization. ACM Comput. Surv. **55**(13s), 1–36 (2023)
48. Qu, P., Faraone, J.N., Evans, J.P., Zheng, Y.-M., Carlin, C., Anghelina, M., et al.: Enhanced evasion of neutralizing antibody response by Omicron XBB. 1.5, CH. 1.1, and CA. 3.1 variants. Cell Reports **42**(5) (2023)
49. Bobrovitz, N., Ware, H., Ma, X., Li, Z., Hosseini, R., Cao, C., et al.: Protective effectiveness of previous SARS-CoV-2 infection and hybrid immunity against the omicron variant and severe disease: a systematic review and meta-regression. Lancet Infect. Dis. (2023)
50. Thompson, R.N., Stockwin, J.E., van Gaalen, R.D., Polonsky, J.A., Kamvar, Z.N., Demarsh, P.A., et al.: Improved inference of time-varying reproduction numbers during infectious disease outbreaks. Epidemics **29**, 100356 (2019)
51. Fu, D., He, G., Li, H., Tan, H., Ji, X., Lin, Z., et al.: Effectiveness of COVID-19 vaccination against SARS-CoV-2 Omicron variant infection and symptoms—China, December 2022–February 2023. China CDC Weekly **5**(17), 369 (2023)
52. Callaway, E.: COVID's future: mini-waves rather than seasonal surges. Nature (2023)
53. Chan, C.X., Yang, Y.O., Cheng, G.H.M., Gera, S.K., Mohammad, A.Z., Oh, S.-J., et al.: Aging and the immune system: the impact of immunosenescence on viral infection, immunity and vaccine immunogenicity. Immune Netw. **11**(4), e37 (2019)
54. Huang, Y., Cai, X., Zhang, B., Zhu, G., Liu, T., Guo, P., Xiao, J., et al.: Spatiotemporal heterogeneity of social contact patterns related to infectious diseases in the Guangdong province, China. Sci. Rep. **10**(1), 6119 (2020)